AMERICAN
METEOROLOGICAL
SOCIETY

Journal of the Atmospheric Sciences

The DOI for this manuscript is doi: 10.1175/JAS-D-11-0308.1

The final published version of this manuscript will replace the preliminary version at the above DOI once it is available.

If you would like to cite this EOR in a separate work, please use the following full citation:

Fuchs, Z., S. Gjorgjievska, and D. Raymond, 2012: Effects of Varying the Shape of the Convective Heating Profile on Convectively Coupled Gravity Waves and Moisture Modes. J. Atmos. Sci. doi:10.1175/JAS-D-11-0308.1, in press.

Effects of Varying the Shape of the Convective Heating Profile on Convectively Coupled Gravity Waves and Moisture Modes

Željka Fuchs[1]

Physics Department, Faculty of Science, University of Split, Split, Croatia; Physics Department and Geophysical Research Center, New Mexico Institute of Mining and Technology, Socorro, New Mexico, 87801 USA

Saska Gjorgjievska and David J. Raymond

Physics Department and Geophysical Research Center, New Mexico Institute of Mining and Technology, Socorro, New Mexico, 87801 USA

[1] *Corresponding author address:* Željka Fuchs, Physics Department and Geophysical Research Center, New Mexico Institute of Mining and Technology, Socorro, New Mexico, 87801. E-mail: zeljka@kestrel.nmt.edu

Abstract

The analytical model of convectively coupled gravity waves and moisture modes of Raymond and Fuchs (2007) is extended to the case of top-heavy and bottom-heavy convective heating profiles. Top-heavy heating profiles favor gravity waves, while bottom-heavy profiles support moisture modes. The latter behavior results from the sensitivity of moisture modes to the gross moist stability, which is more negative with bottom-heavy heating.

A numerical implementation of the analytical model allows calculations in the two-dimensional non-rotating case as well as on a three-dimensional equatorial beta plane. In the two-dimensional case the analytical and numerical models are mostly in agreement, though minor discrepancies occur. In three dimensions the gravity modes become equatorial Kelvin waves while the moisture modes are more complex and require further investigation.

1 Introduction

A generally accepted theory that models the interactions between large-scale motions and deep convection in the tropics is still missing. We are closer to understanding the convectively coupled equatorial waves which correspond in the dry atmosphere to Matsuno's (1966) solutions, but tropical disturbances such as the Madden-Julian oscillation (MJO) and easterly waves are still incompletely understood. Historically it was thought that quasi-equilibrium theory, which assumes that disturbances have a first baroclinic mode form in the vertical can explain the main features of the convectively coupled equatorial waves. Although quasi-equilibrium theory is useful for many applications, today we know that the equatorial waves cannot be characterized only by the first baroclinic mode, but that we need the higher order vertical structure. The open questions are the dynamical role of the vertical structure and to what extent it is important.

Emanuel (1987) introduced a highly simplified form of the convective quasi-equilibrium hypothesis of Arakawa and Schubert (1974) in a linearized model for the MJO. Deep convection is assumed to be near equilibrium with mechanisms which create convective available potential energy (CAPE), while additional processes such as wind-induced surface heat exchange (WISHE) act to destabilize the modes. This model is characterized as implementing strict quasi-equilibrium, since the convection drives the atmosphere instantly to a moist adiabat consistent with the equivalent potential temperature of the boundary layer, which is determined by the interactions of surface fluxes, radiation and vertical motion.

Various models proposed by Yano and Emanuel (1991), Emanuel (1993), Emanuel et al. (1994), Neelin and Yu (1994) follow from a relaxation of strict quasi-equilibrium theory; convective effects are assumed to lag the forcing by the typical convective time scale of a few hours rather than occurring instantaneously. The phase speeds of disturbances with first baroclinic mode vertical structure in quasi-equilibrium with convection are reduced compared with corresponding free adiabatic modes and the modes are damped rather than neutral as in strict quasi-equilibrium. However, the first baroclinic mode structure of simple quasi-equilibrium models, such as those noted above, does not capture the observed complex vertical structure of the temperature, heating and vertical velocity for convectively coupled equatorial Kelvin waves from Straub and Kiladis (2003) and Kiladis et al. (2009).

To solve this problem, Mapes (2000) proposed a two-vertical-mode model where the vertical heating profile is a superposition of deep convective and stratiform parts. The deep convective profile has the structure of the first baroclinic mode, while the stratiform has vertical wavelength half that of the deep mode. The stratiform mode lags the deep convective mode as a result of assumed cloud microphysical processes. Particular significance in the Mapes model is given to the convective inhibition (CIN) closure, without which there are no wave disturbances. When CIN is turned on, the unstable convectively coupled gravity waves have the observed phase speed of convectively coupled Kelvin waves.

Subsequent two-mode models were developed by Majda and Shefter (2001a, b) and Majda et al. (2004). Those models used a lower tropospheric CAPE which bears more relationship to a CIN closure than to the full tropospheric CAPE closure of quasi-equilibrium models. The models developed by Khouider and Majda (2006, 2008) and Kuang (2008) differ from earlier models in that they rely on the effect of midtropospheric humidity to control the depth of convection. This so-called moisture-stratiform mode derives its lag between shallow convection, deep convection, and stratiform conditions from this humidity dependence rather than from cloud microphysical delays in the production of stratiform rain. The moisture–stratiform instability appears to be the main instability mechanism for convectively coupled wave development in the cloud-system-resolving model simulations.

To avoid the quasi-equilibrium and imposed two-vertical-mode assumptions in the above models, Fuchs and Raymond (2007) and Raymond and Fuchs (2007) developed a vertically resolved model that produces the observed complex vertical structure of convectively coupled Kelvin waves assuming a simple, sinusoidal vertical heating profile. The Raymond and Fuchs (RF07) model is a linearized, two-dimensional non-rotating model of the tropical atmosphere which incorporates three crucial factors into its convective closure. These factors, based on the results from observations and numerical models are the importance of convective inhibition (Raymond et al. 2003; Firestone and Albrecht, 1986), the control of precipitation by the saturation fraction or column relative humidity of the troposphere (Bretherton et al., 2004; Sobel et al., 2004; Lucas et al., 2000; Derbyshire et al., 2004; Raymond and Zeng, 2005) and the effects of surface moist entropy fluxes (Raymond et al., 2003; Back and Bretherton, 2005; Maloney and Esbensen 2005). The resulting modes are fast gravity waves, convectively coupled gravity waves and the so-called moisture mode. The moisture mode arises as a consequence of the moisture prognostic equation and is consistent with the results obtained using the weak temperature gradient approximation (WTG) of Sobel et al. (2001) in the limit of zero meridional moisture gradient. Unstable moisture modes arise when two conditions are satisfied: (1) precipitation increases with tropospheric humidity, and (2) convection itself, possibly working with convectively coupled surface flux and radiation anomalies, tends to increase the humidity (Sugiyama, 2009a, b). Though not emphasized by these authors, Neelin and Yu (1994) obtained moisture modes in their linearized quasi-equilibrium model.

RF07 show that two large-scale modes predicted by their model are unstable, a slowly propagating moisture mode which is driven primarily by saturation fraction anomalies and negative effective gross moist stability, and a convectively coupled gravity mode which is governed by anomalies in convective inhibition caused by buoyancy variations just above the top of the planetary boundary layer. The gravity mode is assumed to map onto the equatorial Kelvin wave in the earth's atmosphere and its propagation speed and vertical structure are in agreement with observation (Straub and Kiladis, 2002). Since a CIN closure differs from a lower tropospheric CAPE closure only by the depth range over which parcel buoyancy is taken to control convection, this model is clearly similar to the Khouider and Majda (2006, 2008) and Kuang (2008) models. However, it differs in that it shows that the essential results of these models can be obtained without assuming variation in the vertical heating profile with wave phase.

The disturbances predicted by two-vertical-mode models appear to have the characteristics of convectively coupled Kelvin waves. On the other hand there is increasing evidence that the MJO is in essence a moisture mode (Maloney and Esbensen 2005; Raymond and Fuchs 2009; Sobel et al. 2009).

In this paper we use the same thermodynamics as in RF07, but consider different heating and moisture profiles. In particular, we examine the effects of top and bottom-heavy vertical heating profiles. Moisture profiles are also varied to produce different values of the gross moist stability (GMS). Additionally we develop a numerical version of the model which allows us to expand from two dimensions into a three-dimensional equatorial beta plane, thus allowing rotation to play a role. This enables us to explore the behavior of the unstable modes in a more realistic environment. We find that convectively coupled Kelvin waves are favored by top-heavy heating profiles with positive GMS. In contrast, the unstable moisture modes are produced whenever the GMS is negative. Section 2 develops the modified analytical model equations and section 3 presents the results of the analytical model. The numerical model is developed in section 4 and the results from the model for two and three dimensional cases are given in section 5. Conclusions are drawn in section 6.

2 Analytical model

The linearized, slab symmetric governing equations (horizontal momentum equation, hydrostatic equation, mass continuity and thermodynamic equations for buoyancy b, mixing ratio q and moist entropy e in a non-rotating two-dimensional atmosphere at rest under the Boussinesq approximation are:

$$\frac{\partial u}{\partial t} + \frac{\partial \Pi}{\partial x} = 0 \tag{1}$$

$$\frac{\partial \Pi}{\partial z} - b = 0 \tag{2}$$

$$\frac{\partial u}{\partial x} + \frac{\partial w}{\partial z} = 0 \tag{3}$$

$$\frac{\partial b}{\partial t} + \Gamma_B w = S_B \tag{4}$$

$$\frac{\partial q}{\partial t} + \Gamma_Q w = S_Q \tag{5}$$

$$\frac{\partial e}{\partial t} + \Gamma_E w = S_E \tag{6}$$

In the above equations u is the horizontal wind perturbation, Π is the mean potential temperature times the Exner function perturbation, w is the vertical velocity perturbation. The buoyancy perturbation is defined as $b = gs_d^{'}/T_R$ where $s_d^{'}$ is the perturbation dry entropy that comes from dry entropy being split into mean and perturbation parts $s_d = s_{d0}(z) + s_d'$, g is the acceleration of gravity and $T_R = 300\,\mathrm{K}$ is a constant reference temperature. $\Gamma_B = (g/C_p)ds_{d0}/dz$ is the constant square of the Brunt-Väisälä frequency where C_p is the specific heat of air at constant pressure. The scaled buoyancy source term is $S_B = (g/C_p)ds_d/dt$. The moist entropy perturbation is scaled by g/C_p,

$e = (g/C_p)s'$ where s' is the perturbation moist entropy; $s = s_0(z) + s'$. The scaled moist entropy gradient is $\Gamma_E = (g/C_p)ds_0/dz$ and the scaled moist entropy source term is $S_E = (g/C_p)ds/dt$. The scaled mixing ratio anomaly is given by $q = e - b$, $q = (gL/C_pT_R)r'$, where the mixing ratio $r = r_0(z) + r'$, and L is the latent heat of condensation. The scaled mixing ratio gradient is $\Gamma_Q = (gL/C_pT_R)dr_0/dz$ and the scaled mixing ratio source term is $S_Q = (gL/C_pT_R)dr/dt$.

The equations (1) to (6) lead to an equation for the vertical velocity w

$$\frac{d^2w(z)}{dz^2} + m^2w(z) = \frac{k^2}{\omega^2}S_B(z), \tag{7}$$

and the heating profile is assumed to take the form

$$S_B = Bm_0X\exp(m_0\nu z)\sin(m_0z) \tag{8}$$

where B is the vertically integrated heating anomaly, the quantity into which the thermodynamics of the model will be incorporated. The quantity ν is a dimensionless parameter, $m_0 = \pi/h$, h is the height of the tropopause, and $X = (1+\nu^2)/[1+\exp(\pi\nu)]$. Varying ν from negative to positive values allows us to change the vertical heating profile from bottom-heavy to top-heavy as can be seen from figure 1. $\nu = 0$ brings us back to the neutral or unperturbed heating profile and the results of RF07.

The polarization relations for the buoyancy and the scaled moist entropy perturbation obtained from the equations (4) and (6) respectively are

$$b = (i/\omega)(S_B - \Gamma_B w) \tag{9}$$

$$e = (i/\omega)(S_E - \Gamma_E w) \tag{10}$$

where the x and t dependence take the form $\exp[i(kx - \omega t)]$ with k and ω being the zonal wavenumber and frequency. The vertical wavenumber is $m = k\Gamma_B^{1/2}/\omega$.

The solution to the vertical velocity equation (7) using an upper radiation boundary condition is:

$$\begin{aligned} w(z) = \frac{m_0 BX}{\Gamma_B M_+ M_-} \big[& \left(1 + \Phi^2\nu^2 - \Phi^2\right) \exp\left(m_0 \nu z\right) \sin\left(m_0 z\right) - \\ & 2\nu\Phi^2 \exp\left(m_0 \nu z\right) \cos\left(m_0 z\right) + \\ & 2\nu\Phi^2 \exp\left(-i m_0 z/\Phi\right) - M_+ \Phi \exp\left(\pi\nu - i\pi/\Phi\right) \sin(mz) \big] \end{aligned} \tag{11}$$

where $M_+ = \Phi^2 + (\nu\Phi + i)^2$ and $M_- = \Phi^2 + (\nu\Phi - i)^2$. Substitution of (11) into (9) results in

$$b(z) = \frac{im_0 BX}{\alpha\kappa\Phi M_+ M_-}\Big[(M_+M_- - 1 - \Phi^2\nu^2 + \Phi^2)\exp(m_0\nu z)\sin(m_0 z) +$$
$$2\nu\Phi^2\exp(m_0\nu z)\cos(m_0 z) - \tag{12}$$
$$2\nu\Phi^2\exp(-im_0 z/\Phi) + M_+\Phi\exp(\pi\nu - i\pi/\Phi)\sin(mz)\Big]$$

where $\kappa = h\Gamma_B^{1/2}k/(\pi\alpha)$ is the dimensionless wavenumber and where $\Phi = \omega/(\alpha\kappa) = m_0/m$ is the dimensionless phase speed.

The thermodynamics of the model come into the equations via the vertically integrated heating anomaly which is assumed to depend on the scaled precipitation rate anomaly P and the radiative cooling rate anomaly R:

$$\int_0^h S_B dz = B = P - R = \alpha(1+\varepsilon)\int_0^h q(z)dz + \mu_{CIN}(e_s - e_t) \tag{13}$$

The quantity α is a moisture adjustment rate. The variable ε incorporates the effect of cloud-radiation interactions which are assumed to cause a radiative heating anomaly in phase with precipitation (see Fuchs and Raymond, 2002).

The first term on the right side of (13) is proportional to the precipitable water anomaly. The second term represents the effect of convective inhibition (CIN) on heating. The quantity e_s is the scaled perturbation in boundary layer moist entropy, while e_t is a scaled threshold value of the perturbation moist entropy. The constant μ_{CIN} governs the sensitivity of precipitation rate to deep convective inhibition. We set e_t equal to the saturated moist entropy perturbation at elevation Dh, where D is this elevation expressed as a fraction of the tropopause height h. In the simplified thermodynamic scheme e_t is related to the buoyancy anomaly $b(D)$ at elevation Dh, $b(D)$ by

$$e_t = \lambda_t b(D). \tag{14}$$

The boundary layer moist entropy is subject to a balance primarily between a positive tendency due to surface moist entropy fluxes and a negative tendency due to convective downdrafts and turbulent entrainment of dry air into the boundary layer. In RF07 it was expressed through the simplified assumption that stronger surface wind speeds cause increased surface evaporation, which results in enhanced boundary layer moist entropy anomaly e_s. In this paper we choose to show the results in the absence of wind-induced surface heat exchange (WISHE) which means that we can ignore this term. We show the results without WISHE to simplify the model equations; besides giving an eastward propagation speed to the moisture mode when mean easterlies are imposed, WISHE mechanism does not alter the model results significantly.

Combining (9), (10) and (13) results in an equation for the vertically integrated heating B:

$$B = \frac{i\kappa\Phi + \varepsilon}{1 - i\kappa\Phi}\mu_{CIN}\lambda_t b(D) + \frac{1+\varepsilon}{1 - i\kappa\Phi}(1 - \Gamma_M)\int_0^h \Gamma_B w dz \tag{15}$$

where Γ_M is a version of the gross moist stability of Neelin and Held (1987) which we call the normalized gross moist stability (NGMS; Raymond and Sessions 2007; Raymond et al. 2009):

$$\Gamma_M = \int_0^h \Gamma_E w dz \bigg/ \int_0^h \Gamma_B w dz \ . \tag{16}$$

The integral of the vertical velocity from (11) is:

$$\int_0^h w(z) dz = \frac{B}{\Gamma_B M_+ M_-} F(\Phi) \tag{17}$$

where

$$F(\Phi) = \Phi^2 - 3\Phi^2\chi^2 - 1 + 2i\nu X \Phi^3 \left[1 - \exp(-i\pi/\Phi)\right] + \\ X M_+ \Phi^2 \exp(\pi\nu - i\pi/\Phi) \left[1 - \cos(\pi/\Phi)\right] \tag{18}$$

and the integral that includes the variations in the scaled ambient moist entropy $e_0(z)$ that is assumed to take a piecewise linear form in the troposphere as in FR07 is:

$$\int_0^h \Gamma_E w dz = \frac{B \Delta e X}{M_+ M_-} J(H, \Phi) \tag{19}$$

where

$$
\begin{aligned}
J(H,\Phi) = {} & [H + H\exp(\pi\nu) - 1]\,(1 + 3\Phi^2\nu^2 - \Phi^2)/\left(1+\nu^2\right) - \\
& \nu(1+\Phi^2\nu^2 - 3\Phi^2)\exp(\pi H\nu)\sin(\pi H)/\left(1+\nu^2\right) - \\
& (\Phi^2 - 3\Phi^2\nu^2 - 1)\exp(\pi H\nu)\cos(\pi H)/\left(1+\nu^2\right) + \\
& 2i\nu\Phi^3\left[H\exp(-i\pi/\Phi) - H + 1 - \exp(-i\pi H/\Phi)\right] - \\
& \Phi^2 M_+\exp\left(\pi\nu - \pi i/\Phi\right)\left[H - 1 + \cos\left(\pi H/\Phi\right) - H\cos\left(\pi/\Phi\right)\right].
\end{aligned}
\tag{20}
$$

The NGMS can be expressed:

$$
\Gamma_M = \int_0^h \Gamma_E w dz \bigg/ \int_0^h \Gamma_B w dz = \frac{\Delta e J(H,\Phi)}{XH(1-H)F(\Phi)}. \tag{21}
$$

When $|\Phi|^2 \ll 1$, as is true for all of the interesting modes studied here, it takes the form:

$$
\Gamma_M \approx \frac{\Delta e}{H(1-H)}\left\{H - \frac{1}{1+\exp(\pi\chi\nu)} - \frac{\exp(\pi H\nu)\left[\nu\sin(\pi H) - \cos(\pi H)\right]}{1+\exp(\pi\nu)}\right\} \tag{22}
$$

The parameter H is the fractional height relative to the tropopause of the minimum in the ambient moist entropy profile and $\Delta e = \Delta e_0/h\Gamma_B$ is the scaled difference between the surface and tropopause values of moist entropy (assumed to be the same) and the minimum value at height Hh. Note that this approximate form (22) is real and independent of Φ, which means that Γ_M can be treated as a constant external parameter under these conditions.

Applying the heating closure (13) and combining (11), (18), (15) and (14) results in the dispersion relation for the phase speed Φ:

$$\begin{aligned}
M_+M_-\left(\kappa\Phi + i\right) + 2\chi_t X\left(\varepsilon + i\kappa\Phi\right) L(D,\Phi)/\kappa\Phi + \\
i(1+\varepsilon)(1-\Gamma_M)F(\Phi) = 0.
\end{aligned} \tag{23}$$

The dimensionless parameter $\chi_t = \lambda_t \mu_{CIN} m_0/(2\alpha)$ represents the sensitivity of precipitation to the degree of convective inhibition while the auxiliary function $L(D,\Phi)$ is defined as:

$$\begin{aligned}
L(D,\Phi) = \left(M_+M_- - 1 - \Phi^2\nu^2 + \Phi^2\right)\exp(\pi\nu D)\sin(\pi D) + \\
2\nu\Phi^2\exp(\pi\nu D)\cos(\pi D) - 2\nu\Phi^2\exp\left(-i\pi D/\Phi\right) + \\
M_+\Phi\exp\left(\pi\nu - i\pi/\Phi\right)\sin(\pi D/\Phi).
\end{aligned} \tag{24}$$

The dispersion relation given by (23) is transcendental and has to be solved numerically using Newton's method.

3 Analytical model results

3.1 Control case

The parameters used to calculate the dispersion curves in figure 2 were discussed at length in RF07 and their values are given in table 1. These parameters are: cloud-radiation interaction (CRI) parameter ε, scaled height of moist entropy minimum H, scaled magnitude of entropy minimum Δe, scaled height of CIN threshold layer D, sensitivity to convective inhibition χ_t and gross moist stability NGMS. The sensitivity to the vertical heating profile parameter is expressed via parameter ν. The control case has $\nu = 0$ as in RF07 which means that the heating profile is unperturbed, i.e., neither top nor bottom-heavy.

The upper panel of figure 2 shows the phase speed $\mathrm{Re}(\omega/k)$ in meters per second while the bottom panel shows the growth rate $\mathrm{Im}(\omega)$ in units of 1/day. The phase speed and the growth rate are shown as a function of planetary wavenumber l defined as the circumference of the earth divided by the zonal wavelength. There are 3 types of modes, one that corresponds to a fast gravity wave, eastward and westward propagating with a phase speed of 48 m/s and decaying, a convectively coupled gravity wave propagating eastward and westward with a phase speed of about 18 m/s and growing in time, and the moisture mode that is also growing in time. The convectively coupled gravity wave has a maximum growth rate for the planetary wavenumber $l = 7$ which together with the phase speed of 18 m/s agrees well with the observations (Wheeler and Kiladis, 1999, Straub and Kiladis, 2002). The moisture mode is stationary when there are no mean easterlies present and slowly propagates eastward in the presence of surface mean easterlies under the influence of WISHE (not shown here).

From RF07 we know that the convectively coupled Kelvin wave is unstable due to variations in CIN correlated with convection, while the moisture mode is unstable due to cloud radiation interactions and negative gross moist stability, i.e. when the effective gross moist stability is negative.

3.2 Variations in vertical heating and moisture profile

We now explore how changes in the heating and moisture profiles affect the unstable modes from figure 2, i.e. the convectively coupled gravity wave and the moisture mode. The heating profile is varied from top-heavy to bottom-heavy by varying the nondimensional parameter ν. Positive ν corresponds to a top-heavy heating profile, negative to bottom-heavy, while $\nu = 0$ corresponds to the unmodified heating profile of RF07. The values used are given in figure 1. The moisture profile is varied to yield different values of the gross moist stability for a fixed value of ν.

Figure 3 shows convectively coupled gravity wave dispersion curves for different heating profiles. It is clear that the growth rate is highly dependent on the heating profile. The gravity mode is strongly unstable for the top-heavy heating profile while decaying for bottom-heavy one. The wavelength of the maximum growth rate shifts as well; for the top-heavy heating profile the maximum growth rate occurs at larger planetary wavenumber, $l = 12$, while in the control case it occurs at $l = 7$. The phase speed increases from 17 m/s for the bottom-heavy to 21 m/s for the top-heavy heating profile. As the physical mechanism responsible for destabilizing the convectively coupled gravity wave is variations in CIN, we now vary χ_t while keeping the heating profile fixed. Figure 4 shows the dispersion curves for the top-heavy heating profile. Each curve corresponds to a different χ_t value; $\chi_t = 12$ was the value taken in a control case. The mode is unstable for a range of χ_t values, i.e. for $\chi_t \geq 1$. The shift of the maximum growth rate to larger planetary wavenumbers is notable as χ_t values become larger. Varying the moisture profile via different values of NGMS shows that the unstable convectively coupled gravity waves are not sensitive to NGMS per se. However, they are more likely to occur when NGMS is positive since positive NGMS is generally correlated with the top-heavy heating profiles (see table 2).

Figure 5 shows the growth rate of the moisture mode when the heating profile is varied and NGMS is fixed to $\Gamma_M = -0.1$. We ignore CIN as unimportant to the development of the moisture mode. The moisture modes with the same NGMS develop regardless of the shape of the heating profile. This can be understood if we take the limit of non-dimensional phase speed $|\Phi^2| \ll 1$, which is true for the moisture modes, from the equation (23). The dispersion relation (23) then approximately reduces to $\Phi = i\left(\varepsilon - \Gamma_M\right)/\kappa$ and there is no direct dependence on the ν parameter, i.e. on the vertical heating profile. This is also consistent with the results obtained using the WTG approximation (Sobel et al., 2001); in the context of our model, WTG is equivalent to setting the buoyancy perturbation $b = 0$ in the governing equations. We conclude that when the effective NGMS, $\Gamma_M - \epsilon$, is less then zero, the moisture mode is unstable. Figure 6 shows the growth rate of the moisture mode when the moisture profile is varied to change the NGMS and the heating profile is bottom-heavy. As expected, more negative NGMS values result in more unstable modes. To summarize, in the real atmosphere, unstable moisture modes are expected when effective NGMS is negative, with their growth rates becoming larger when effective NGMS is more negative (see table 2).

3.3 Vertical structure

Figure 7 shows the vertical structure of the eastward moving convectively coupled gravity wave in the $x - z$ plane. The left and right panels show respectively the buoyancy anomalies at the planetary wavenumber of maximum growth rate for the unmodified heating profile and the top-heavy vertical heating profile. For both vertical heating profiles the characteristic boomerang structure with westward-tilting contours of positive buoyancy anomaly in the low to middle troposphere and eastward tilt above is seen. This matches the findings from observations (Wheeler et al., 2000, Straub and Kiladis, 2002) and from cloud resolving numerical simulations (Peters and Bretherton, 2006, Tulich et al., 2007). The westward tilting contours of buoyancy anomaly reach a bit higher in the case of top-heavy heating profile.

Figure 8 shows the vertical structure of the moisture mode for planetary wavenumber $l = 2$ in the $x - z$ plane. It shows the buoyancy anomalies and the convective heating for the unmodified and bottom-heavy heating profile. The buoyancy anomalies are in phase with heating as the mode is stationary and there is no tilted structure.

The vertical structure of the moisture mode is very different from that of the convectively coupled gravity wave. The buoyancy anomaly contours are arbitrary in figures 7 and 8, but their ratio to the heating is fixed. We can use that ratio to evaluate the relative magnitude of the temperature anomaly between the two unstable modes. It turns out that the ratio between the buoyancy and heating for the convectively coupled Kelvin waves is an order of magnitude larger than for the moisture mode, confirming that in its essence the moisture mode is a weak temperature gradient mode (Sobel et al. 2001, Sobel and Bretherton, 2003).

4 Numerical model

The dynamical core of the numerical model follows the model of Raymond and Fuchs (2009). It is cast in sigma isentropic coordinates, i.e., the vertical coordinate is defined in terms of the potential temperature θ:

$$\sigma = (\theta - \theta_B)/(\theta_T - \theta_B) \tag{25}$$

where θ_T is the (constant) potential temperature at the top of the domain and θ_B is the (possibly variable) temperature at the bottom of the domain. When θ_B is taken to be constant, the vertical coordinate mimics isentropic coordinates. The model can be run on an f plane or on a β plane. It is periodic in the longitudinal direction, while in the latitudinal direction it can be either periodic or bounded by rigid walls (channel model). The top layer of the domain is a sponge layer. Its purpose is to absorb upward-moving waves, thus emulating an upward radiation boundary condition. Though the dynamics of the model are fully nonlinear we only analyze results with small amplitude flow perturbations, making the model effectively linear. For further information on the dynamics, see Raymond and Fuchs (2009).

The thermodynamics of the model is similar to that of the analytical model described above. Since the implementation of the thermodynamics is done in the context of a non-Boussinesq numerical calculation, we repeat the presentation in the new context. The perturbation precipitation is calculated from:

$$P = \alpha(W - W_m) - \mu_{cin}\left(\frac{\rho_R C_p}{L}\right)[\theta'_{es}(d) - \theta'_e(0)]. \tag{26}$$

W is the precipitable water and W_m is the vertical mean value of this quantity. If precipitable water is bigger than the mean precipitable water, the result is a positive rainfall perturbation and vice versa. The quantity α is the moisture relaxation constant that regulates the strength of the precipitable water control on the rainfall as in the analytical model. $\theta'_{es}(d)$ is the perturbation saturated equivalent potential temperature above the boundary layer at height d and $\theta'_e(0)$ is perturbation of equivalent potential temperature at the surface. Note that in the analytical model we use the moist entropy perturbation while in the numerical model we use the equivalent potential temperature perturbation. In all other aspects the precipitation closure is the same. The parameter μ_{CIN} governs the sensitivity of precipitation rate to CIN and ρ_R is the air density of boundary layer air.

The vertical profile of the heating, i.e., the potential temperature perturbation source, takes the form:

$$S_\theta = B \sin(m_0 z) \exp(\nu z) \Big/ \int_0^{\sigma_t} \eta(\sigma) \sin(m_0 z) \exp(\nu z) \, d\sigma \;, \tag{27}$$

where the vertically integrated heating is

$$B = L(P - R)/C_p, \tag{28}$$

with R being the radiative cooling perturbation. As in the analytical model, it is assumed to be proportional to minus the moisture-induced precipitation rate:

$$R = -\varepsilon\alpha(W - W_m). \tag{29}$$

The parameter ε is called cloud-radiative feedback parameter and for our numerical simulations it takes the value of 0.2 as is the case in the analytical model. The parameter $m_0 = \pi/h$, where h is the depth of the troposphere, η is the density in the sigma isentropic coordinate system and z is the geometrical height. The skew parameter ν determines the height at which the maximum heating perturbation will occur. For $\nu = 0$ it takes form of the first baroclinic mode, as in the analytical model.

The moisture perturbation source is:

$$S_r = (E - P) \exp(-z/z_q) \Big/ \int_0^{1} \eta \exp(-z/z_q) d\sigma \;, \tag{30}$$

where z_q is the scale height of water vapor. E stands for evaporation rate anomaly and it is parametrized to be proportional to the background zonal wind in the boundary layer. However, the simulation results presented in this paper are done with zero background wind and therefore the surface fluxes are shut off ($E = 0$). As a consequence, $\theta_e^{'}(0)$ in equation (26) is equal to zero and the CIN variations are entirely due to variations in the saturated equivalent potential temperature above the boundary layer.

As noted above, there are two distinct mechanisms that are responsible for the two unstable modes of RF07. One is associated with variations of CIN, mainly variations of the saturated equivalent potential temperature or the saturated moist entropy just above the boundary layer. The other mechanism is related to small or negative GMS. For the analysis in the numerical model we use a normalized form of the gross moist stability (NGMS) from Raymond et al. (2009) defined in the sigma isentropic coordinates as

$$\Gamma_R = -\frac{C_p \int_0^1 \eta S_\sigma (\partial \theta_e / \partial \sigma) d\sigma}{L \int_0^1 \eta S_\sigma (\partial r_t / \partial \sigma) d\sigma} \tag{31}$$

where r_t is the total mixing ratio and $S_\sigma = d\sigma/dt$ is the vertical velocity in the vertical coordinate of the numerical model. As Raymond et al. (2009) show, this form of the NGMS is essentially equivalent to (16). Furthermore, both are equivalent to the NGMS used by Raymond and Fuchs (2009) when the horizontal advection of equivalent potential temperature and moisture are neglected, as is justified in the linearized models used in this paper.

From (31) it is evident that a change in either the heating or the moisture profile will change the value of NGMS. Figure 9 shows the variety of heating perturbation profiles (left panel) and moisture perturbation profiles (right panel) used for the simulations. The values are scaled, but show the height at which the maximum heating perturbations occur and how slowly the mixing ratio decreases with height. The height of the troposphere is taken to be 15km. Note that some of the moisture profiles that are used are idealized, in a sense that such slow decreases of the water vapor with height are impossible in the earth's atmosphere, as supersaturation would occur in the upper troposphere. We use them only to obtain a wide range of NGMS values.

As we compare the results of the numerical model with the results from the analytical model, two things should be noted about their differences. First, the dynamics of the two models are different; the analytical model uses the Boussinesq approximation, while the numerical model represents the full set of primitive equations. Second, the solution methods are different. In particular, for given values of the CIN parameter and NGMS, the analytical model calculates a dispersion relation. Thus, the growth rates and the phase speeds are calculated for a range of wavenumbers. In the numerical model the wavenumber cannot be externally specified, and a dispersion curve cannot be constructed. A numerical solution for given heating and moisture profiles gives only the most unstable mode, i. e., the peak of the dispersion curve. We find that the wavelength and the period of the resulting disturbances are sensitive to the spatial resolution of the model, and are therefore not very robust. However, the phase speeds and the growth rates of modes are not sensitive to model details, which gives us more confidence in the results for these parameters. Thus, for the purpose of comparing the numerical and analytical model results we use the phase speed and the growth rate.

Each numerical simulation is initiated by applying random density perturbations. The model is then run for three and a half months. The initial perturbations are very small (fractional density 10^{-6}) in order to allow the most unstable modes to emerge while maintaining linearity. For this reason, disturbances take a long time to develop and the simulations have very long run-times. The analysis is restricted to periods with small amplitudes of the resulting disturbances.

5 Numerical model results

5.1 Two-dimensional cases

In this section we make comparisons between the analytical and numerical model results. The numerical model is run in two-dimensional, non-rotating mode with zero background wind. The computational domain is 12000 km in the horizontal and 22 km in the vertical, with the tropopause set to 15 km. The horizontal grid size is 100 km and 40 levels equally spaced in σ are defined in the vertical. A time step of 100 s is used. The vertical gradient of the potential temperature $d\theta/dz$ is the same in both the troposphere and stratosphere and is taken to be 3.3 K/m, which corresponds to a Brunt–Väisälä frequency of 10^{-2} s^{-1}. The rest of the parameters are the same as in the analytical model, shown in table 1. A series of simulations is performed where each simulation has a prescribed unique combination of the heating and moisture profiles shown in figure 9.

The first set of simulations corresponds to the case in which only CIN variations are allowed, i. e., $\alpha = 0$. In the analytical model this set of parameters produces only convectively coupled gravity waves. The same holds true for the numerical model results.

Figure 10 shows the phase speed and growth rate of the most unstable convectively coupled gravity wave as a function of the height of the level of maximum heating rate. The lines indicate least-squares fits to the numerical results. As in the case of the analytical model, the phase speed and growth rate both increase with the level of maximum heating. This demonstrates that convectively coupled gravity waves are favored by top-heavy convective heating profiles. The results presented in this case are insensitive to changes in the moisture profiles. This demonstrates that the convectively coupled gravity waves are insensitive to changes in the NGMS, since this quantity depends on both the environmental moisture profile (via its effect on the moist entropy profile) and on the heating profile. This invariance is explained by (26). Provided that $\alpha = 0$, only changes in the saturated equivalent potential temperature above the boundary layer should affect the characteristics of the resulting modes. Since θ_{es} at this level is only a function of temperature, varying the mixing ratio does not change the result.

Another set of simulations was done to determine how sensitive the wave characteristics are to changes in the parameter μ_{CIN} (results not shown). All the runs had the same top-heavy heating profile, but different values for μ_{CIN}. For larger values of μ_{CIN} the resulting gravity waves had larger growth rates but the same phase speed, which agrees with the results from the analytical model.

An analogous series of simulations was performed with $\alpha \neq 0$ and $\mu_{CIN} = 0$. In cases where the NGMS is very small or negative, moisture modes develop. They are always stationary, provided that there is no background flow. The growth rates of these modes depend only on the NGMS. Thus, in two simulations initiated with different heating and moisture profiles but the same NGMS, moisture modes with the same growth rates develop. Generally, for physically realistic moisture profiles, bottom-heavy heating profiles must be invoked to produce negative NGMS.

Figure 11 gives the growth rate of the moisture mode as a function of NGMS. As the figure shows, simulations with more negative NGMS result in moisture modes with faster growth rates. There are no developing moisture modes in simulations with NGMS larger then 0.04.

Simulations initiated with a top-heavy heating profile in this case sometimes produce weakly intensifying convectively coupled gravity waves even though $\mu_{CIN} = 0$. The destabilizing mechanism for these modes is rather mysterious. Top-heavy heating profiles exhibit large positive NGMS values and therefore the mechanism that drives moisture modes is absent. In addition the CIN control is explicitly turned off. Furthermore, when CIN control is gradually introduced, these modes evolve into normal convectively coupled gravity modes. We suspect that these modes are destabilized as a result of inaccuracies in their numerical representation, but we have been unable to track down the exact mechanism. In any rate, their growth rates are significantly smaller than the convectively coupled modes which develop when $\mu_{CIN} \neq 0$.

Simulations where both the precipitable water anomaly and the CIN parameter are allowed to control the precipitation perturbation were performed (results not shown). Bottom-heavy heating profiles resulted in unstable moisture modes while top-heavy heating profiles led to unstable convectively coupled gravity waves. More precisely, gravity modes occur when the NGMS is positive and moisture modes prevail when it is negative.

5.2 Three-dimensional cases

Three-dimensional simulations were investigated to extend the reach of our analytical model to the case of a rotating environment. We are interested in whether any fundamentally new types of unstable modes appear in three dimensions, and how the third dimension changes the characteristics of the modes we see in two dimensions.

The model is run in channel mode on an equatorial beta plane. The domain size is 12000 km in longitudinal direction, 6000 km in the latitudinal direction, centered on the equator, and 22 km in the vertical with the tropopause at 15 km. The horizontal resolution is 100 km in both directions, there are 40 levels in the vertical and the time-step is 0.1 ks. Throughout the troposphere the Brunt–Väisälä frequency is 10^{-2} s^{-1} and 1.4×10^{-2} s^{-1} in the stratosphere. There are sponge layers on the north-south boundaries and a cyclic boundary condition is applied in the east-west direction. A sponge layer also exists at the top of the domain as in the two-dimensional simulations. For all the simulations the sea surface temperature is constant in space and time. We examine linear perturbations on a base state at rest.

To analyze the behavior of convectively coupled gravity waves in three dimensions, we perform a series of simulations with $\mu_{CIN} \neq 0$ and $\alpha = 0$. The parameters used for the three dimensional calculation are the same as in two-dimensional case. The convectively coupled waves take on the latitudinal structure of equatorial Kelvin waves moving to the east as figure 12 shows. As expected, there is no westward-moving wave component. The phase speeds and the growth rates are similar to those in the two-dimensional case. As in the two-dimensional case, the waves are most unstable and propagate most rapidly with top-heavy heating profiles. The Kelvin wave in the illustrated case has a wavelength of about 7000 km, a latitudinal scale of about 1000 km, a propagation speed of roughly 22 m/s, and a growth rate of approximately 0.45 day^{-1}. The vertical structure is similar to that obtained from the analytical model, figure 13.

The results for the moisture mode in three-dimensional calculations are more complex than in the two-dimensional case (see figure 14). The two-dimensional results are similar to those from the analytical model, with the heating and potential temperature anomalies in phase. This does not occur in the three-dimensional calculations, most likely due to the beta effect. The vertical structure of the temperature anomaly differs somewhat between the analytical and numerical results. However, consistent with WTG, the magnitude of the temperature anomaly is very small in both cases. The three-dimensional case requires further investigation.

6 Conclusions

In RF07 we demonstrated that two types of large-scale tropical modes, convectively coupled gravity waves and moisture modes, arise from two different convective forcing mechanisms, namely, coherent variations in CIN correlated with convection and a moisture feedback mechanism associated with small or negative values of gross moist stability. This work is highly idealized in the sense that the vertical heating profile is specified to have a sinusoidal, first baroclinic mode shape, suggesting that the essential dynamics of these modes are determined more by the gross atmospheric response to heating rather than the detailed structure of the heating pattern.

In the present work we extend these results to the case in which the heating profile ranges from top-heavy to bottom-heavy, with maximum heating in the upper and lower troposphere respectively. We demonstrate that top-heavy heating profiles favor convectively coupled gravity waves whereas bottom-heavy profiles favor moisture modes. The results regarding convectively coupled waves are in agreement with those of Kuang (2010) and Tulich and Mapes (2010). These authors characterize their convective control as a "shallow CAPE", but this is physically very similar to our "deep CIN".

The moisture modes respond more to the value of the NGMS than to the shape of the heating profile per se. Bottom-heavy heating profiles favor the moisture mode simply because those profiles tend to produce small values of NGMS. However, the imposition of unrealistic thermodynamic structures which result in small NGMS even with top-heavy heating profiles produces moisture mode instability, demonstrating that NGMS is the real controlling factor.

In addition to the new analytical results, we have also made two and three-dimensional numerical calculations on an equatorial beta plane using a numerical implementation of our analytical convective heating model. The two-dimensional calculations are mostly in agreement with the analytical results. Minor discrepancies are probably attributable to differences in model dynamics (full primitive equations vs. Boussinesq approximation) and the inevitable errors that arise from modeling a continuous process on a finite grid.

In three dimensions the convectively coupled gravity waves become convectively coupled equatorial Kelvin modes with their characteristic structure. The moisture modes take on a complex structure in the three-dimensional case, which we do not investigate further here.

Acknowledgments. The authors thank the reviewers George Kiladis and Adam Sobel for their useful input. This work was supported by U. S. National Science Foundation Grant ATM1021049.

REFERENCES

Arakawa, A. and W. H. Schuber. 1974: Interaction of a cumulus cloud ensemble with the large-scale environment, Part I. *J. Atmos. Sci.,* **31**, 674-701.

Back, L. E. and Bretherton, C. S. 2005: The relationship between wind speed and precipitation in the Pacific ITCZ. *J. Climate,* **18,** 4317-4328.

Bretherton, C. S., Peters, M. E. and Back, L. E. 2004: Relationships between water vapor path and precipitation over the tropical oceans. *J. Climate,* **17,** 1517-1528.

Derbyshire, S. H., Beau, I., Bechtold, P., Grandpeix, J.-Y., Piriou, J.-M., Redelsperger, J.-L. and Soares, P. M. M. 2004: Sensitivity of moist convection to environmental humidity. *Quart. J. Roy. Meteor. Soc.,* **130,** 3055-3079.

Emanuel, K. A. 1987: An air-sea interaction model of intraseasonal oscillations in the tropics. *J. Atmos. Sci.,* **44,** 2324-2340.

Emanuel, K. A. 1993: The effect of convective response time on WISHE modes. *J. Atmos. Sci.,* **50,** 1763-1775.

Emanuel, K. A., J. D. Neelin, and Bretherton C. S., 1994: On large-scale circulations in convecting atmospheres. Quart. J. Roy. Meteor. Soc., 120, 1111–1143.

Firestone, J. and Albrecht, B. A. 1986: The structure of the atmospheric boundary layer in the central equatorial Pacific during FGGE. *Mon. Wea. Rev.,* **114,** 2219-2231.

Fuchs, Ž. and Raymond, D. J. 2002: Large-scale modes of a nonrotating atmosphere with water vapor and cloud-radiation feedbacks. *J. Atmos. Sci.,* **59,** 1669-1679.

Fuchs, Ž. and Raymond, D. J. 2007: A simple, vertically resolved model of tropical disturbances with a humidity closure. *Tellus*, **59A**, 344-354.

Khouider, B. and Majda, A. J. 2006: A simple multicloud parameterization for convectively coupled tropical waves. Part I: Linear analysis. *J. Atmos. Sci.*, **63**, 1308-1323.

Khouider**,** B., and Majda, A. J. 2008: Multi-cloud models for organized tropical convection: Enhanced congestus heating. *J. Atmos. Sci.*, **65**, 895 – 914.

Kuang, Z. 2008: A moisture-stratiform instability for convectively coupled waves. *J. Atmos. Sci.*, **65**, 834-854.

Kuang, Z. 2010: Linear Response Functions of a Cumulus Ensemble to Temperature and Moisture Perturbations and Implications for the Dynamics of Convectively Coupled Waves. *J. Atmos. Sci.*, **67**, 941-962.

Kiladis, G. N., M. C. Wheeler, P. T. Haertel, K. H. Straub, and P. E. Roundy. 2009: Convectively coupled equatorial waves, *Rev. Geophys.*, **47**, RG2003, DOI 10.1029/2008RG000266.

Lucas, C., Zipser, E. J. and Ferrier, B. S. 2000: Sensitivity of tropical west Pacific oceanic squall lines to tropospheric wind and moisture profiles. *J. Atmos. Sci.,* **57,** 2351-2373.

Majda, A. J., Khouider, B., Kiladis, G. N., Straub, K. H. and Shefter, M. G. 2004: A model for convectively coupled tropical waves: Nonlinearity, rotation, and comparison with observations. *J. Atmos. Sci.,* **61,** 2188-2205.

Majda, A. J. and Shefter, M. G. 2001a: Waves and instabilities for model tropical convective parameterizations. *J. Atmos. Sci.,* **58,** 896-914.

Majda, A. J. and Shefter, M. G. 2001b: Models for stratiform instability and convectively coupled waves. *J. Atmos. Sci.,* **58,** 1567-1584.

Maloney, E. D., and S. K. Esbensen, 2005: A modeling study of summertime east Pacific wind-induced ocean-atmosphere exchange in the intraseasonal oscillation. *J. Climate*, **18,** 568-584.

Mapes, B. E. 2000: Convective inhibition, subgrid-scale triggering energy, and stratiform instability in a toy tropical wave model. *J. Atmos. Sci.,* **57**, 1515-1535.

Matsuno, T. 1966: Quasi-geostrophic motions in the equatorial area. *J. Meteor. Soc. Japan,* **44,** 25-43.

Neelin, J. D. and Held, I. M. 1987: Modeling tropical convergence based on the moist static energy budget. *Mon. Wea. Rev.,* **115,** 3-12.

Neelin, J. D. and Yu, J.-Y. 1994: Modes of tropical variability under convective adjustment and the Madden-Julian oscillation. Part I: Analytical theory. *J. Atmos. Sci.,* **51,** 1876-1894.

Peters, M. E. and Bretherton, C. S. 2006: Structure of tropical variability from a vertical mode perspective. *Theor. Comput. Fluid Dyn.*, **20**, 501-524, DOI 10.1007/s00162-006-0034-x.

Raymond, D. J., Raga, G. B., Bretherton, C. S. , Molinari, J., López-Carrillo, C. and Fuchs, Ž. 2003: Convective forcing in the intertropical convergence zone of the eastern Pacific. *J. Atmos. Sci.,* **60,** 2064-2082.

Raymond, D. J. and Zeng, X. 2005: Modeling tropical atmospheric convection in the context of the weak temperature gradient approximation. *Quart. J. Roy. Meteor. Soc.,* **131,** 1301-1320.

Raymond, D. J. and Fuchs, Ž. 2007: Convectively coupled gravity and moisture modes in a simple atmospheric model. *Tellus*, **59A**, 627-640.

Raymond, D. J. and Fuchs, Ž. 2009: Moisture modes and the Madden-Julian oscillation. *J. Climate*, **22**, 3031-3046.

Raymond, D. J. and Sessions, S. L. 2007: Evolution of convection during tropical cyclogenesis. *Geophys. Res. Letters*, **34**, L06811, doi:10.1029/2006GL028607.

Raymond, D. J., Sessions, S. L., Sobel, A. H. and Fuchs, Ž. 2009: The mechanics of gross moist stability. *JAMES*, **1**, doi:10.3894/JAMES.2009.1.9.

Sobel, A. H., Nilsson J. and Polvani L. M., 2001: The weak temperature gradient approximation and balanced tropical moisture waves. *J. Atmos. Sci.*, **58**, 3650-3665.

Sobel, A. H. and Bretherton, C. S. 2003: Large-scale waves interacting with deep convection in idealized mesoscale model simulations. Tellus, **55A**, 45-60.

Sobel, A. H., Yuter, S. E., Bretherton, C. S. and Kiladis, G. N. 2004: Large-scale meteorology and deep convection during TRMM KWAJEX. *Mon. Wea. Rev.,* **132,** 422-444.

Straub, K. H. and Kiladis, G. N. 2002: Observations of a convectively coupled Kelvin wave in the eastern Pacific ITCZ. *J. Atmos. Sci.,* **59,** 30-53.

Straub, K. H. and Kiladis, G. N. 2003: The observed structure of convectively coupled Kelvin waves: Comparison with simple models of coupled wave instability. *J. Atmos. Sci.,* **60**, 1655-1668.

Sugiyama, M. 2009a: The moisture mode in the quasi-equilibrium tropical circulation model. Part I: Analysis based on the weak temperature gradient approximation. *J. Atmos. Sci.,* **66**, 1507-1523.

Sugiyama, M. 2009b: The moisture mode in the quasi-equilibrium tropical circulation model. Part II: Nonlinear behavior on an equatorial beta plane. *J. Atmos. Sci.,* **66**, 1525-1542.

Tulich, S. N., Randall, D. A. and Mapes, B. E. 2007: Vertical-mode and cloud decomposition of large-scale convectively coupled gravity waves in a two-dimensional cloud-resolving model. *J. Atmos. Sci.,* **64**, 1210-1229.

Tulich, S. N. and Mapes, B. E. 2010: Transient environmental sensitivities of explicitly simulated tropical convection. *J. Atmos. Sci.*, **67**, 957–974.

Wheeler, M., Kiladis, G. N. and Webster, P. J. 2000: Large-scale dynamical fields associated with convectively coupled equatorial waves. *J. Atmos. Sci.,* **57,** 613-640.

Wheeler, M. and Kiladis, G. N. 1999: Convectively coupled equatorial waves: Analysis of clouds and temperature in the wavenumber-frequency domain. *J. Atmos. Sci.,* **56,** 374-399.

Yano, J.-I. and Emanuel, K. A. 1991; An improved model of the equatorial troposphere and its coupling with the stratosphere. *J. Atmos. Sci.,* **48,** 377-389.

List of Tables

Table 1: Control case: non-dimensional free parameters used in calculation of the dispersion relation 23.

Parameter	Value	Comment
ε	0.2	cloud-radiation interaction
H	0.5	scaled height of moist entropy minimum
Δe	0.26	scaled magnitude of entropy minimum
D	0.17	scaled height of CIN threshold layer
χ_t	12	sensitivity to stable layers
Γ_M	0	gross moist stability
ν	0	sensitivity to vertical heating profile

Table 2: NGMS values Γ_M from equation (22) for different vertical heating profiles and for different height levels of the minimum moist entropy.

$\nu \setminus H$	1/3	1/2	2/3
0.5	0.21	0.14	0.04
0	0.1	0	-0.1
-0.5	-0.04	-0.14	-0.21

List of Figures

and dashed lines negative. Left panel shows the unmodified heating profile and right panel shows top-heavy vertical heating profile.

8. As in figure 7, heating anomaly and buoyancy perturbation, only for the moisture mode. Left panel shows the unmodified heating profile and right panel shows bottom-heavy vertical heating profile.

9. Scaled heating (left panel) and moisture (right panel) profiles as a function of height used for numerical model runs.

10. Left panel shows the phase speed for the convectively coupled gravity waves as a function of maximum heating height while right panel shows their growth rate.

11. Growth rate for a moisture mode as a function of NGMS.

12. Convectively coupled Kelvin wave: left panel shows a snapshot of rainfall perturbations at the surface while right panel shows Hövmoller diagram of rainfall at the equator. The bold lines are zero contours, solid lines represent positive values and dashed lines represent negative values.

13. Vertical structure of the convectively coupled Kelvin wave along the equator in the numerical model. The heating anomaly is given in shading and potential temperature perturbation in contours. Light shading represents positive heating anomaly and dark negative. Solid contours represent positive potential temperature anomalies and dashed contours negative anomalies.

14. Heating anomaly and potential temperature as in figure 13, except for the moisture mode. The left panel shows vertical structure of the moisture mode in the two-dimensional case. The right panel shows the vertical structure along the equator in the three-dimensional case.

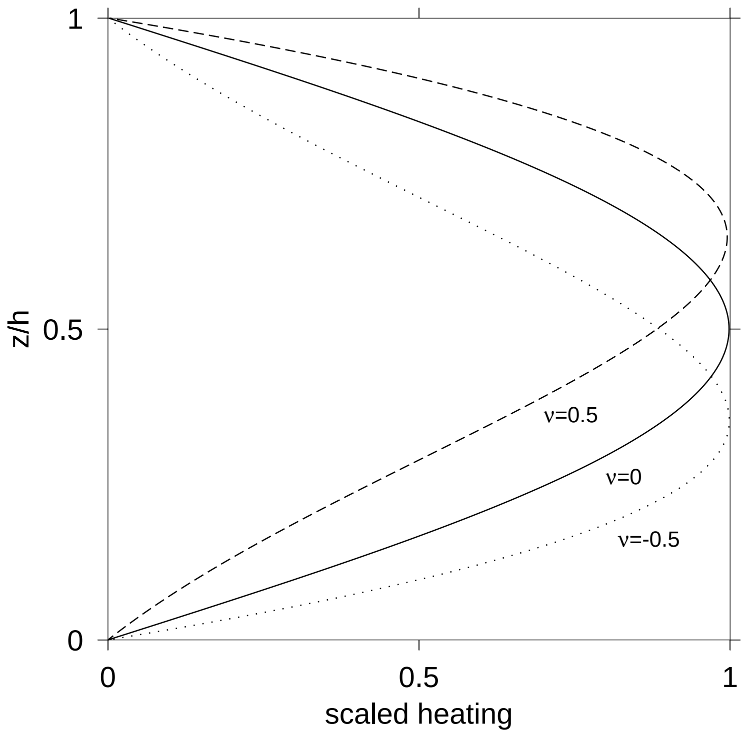

Figure 1: Scaled heating profile as a function of scaled height for different values of ν. Negative ν produces bottom-heavy heating profiles while positive ν produces top-heavy profiles.

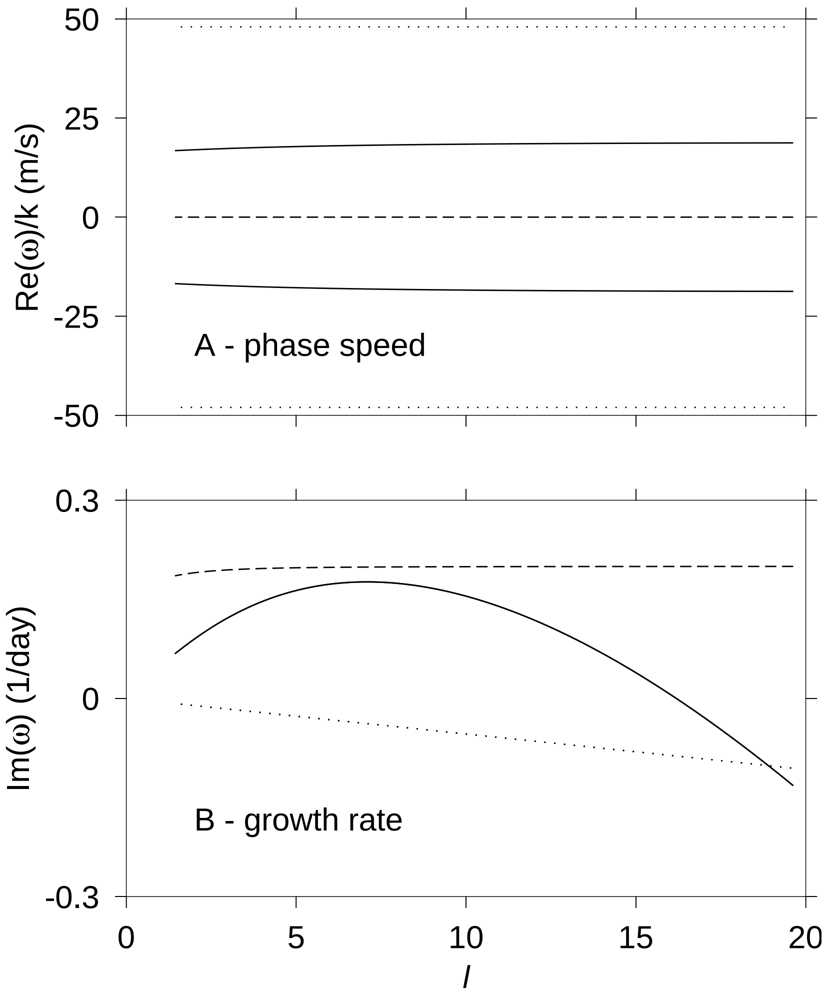

Figure 2: Real part of phase speed (upper panel) and imaginary part of frequency (lower panel) for control case (see table 1). The solid lines show convectively coupled gravity waves, dotted lines show fast gravity waves, and dashed lines show the moisture mode.

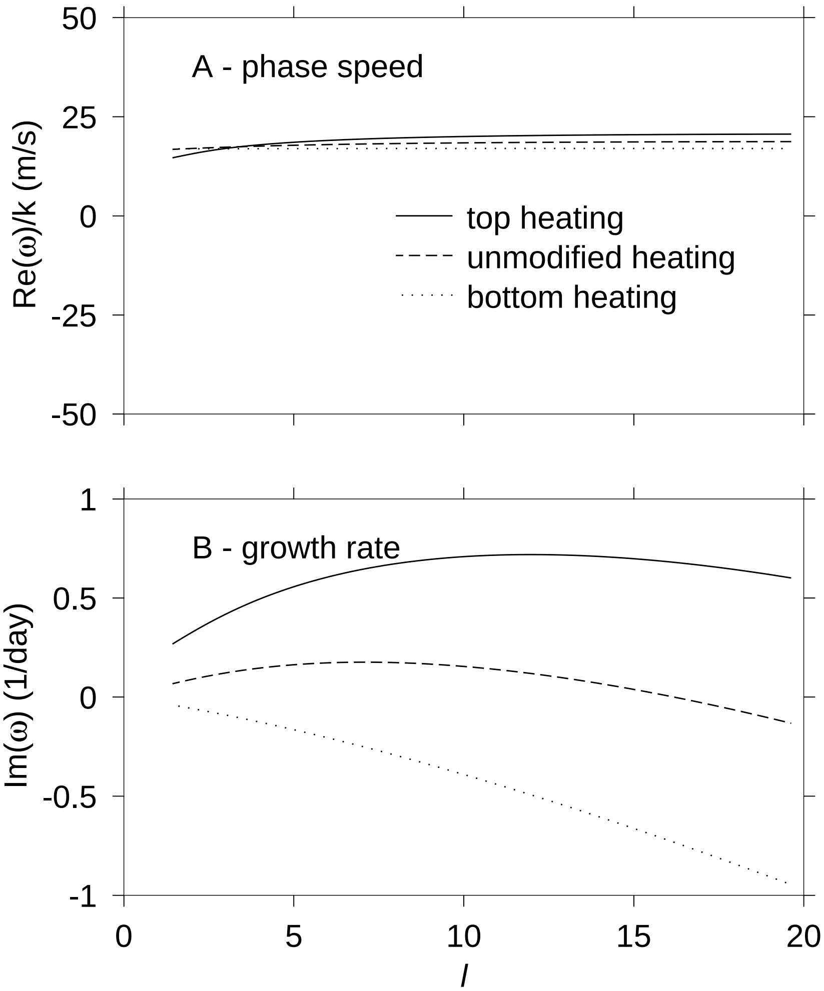

Figure 3: Convectively coupled gravity wave for top, unmodified and bottom-heavy heating profile.

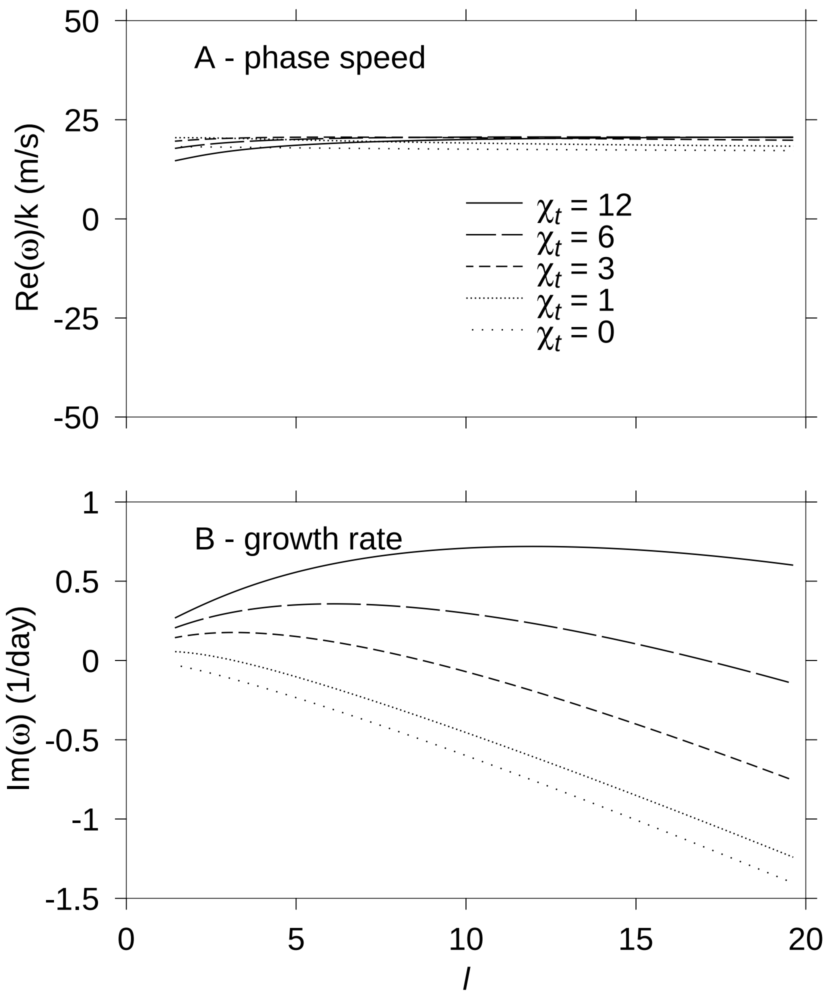

Figure 4: Convectively coupled gravity wave for different χ_t values for top-heavy vertical heating profile.

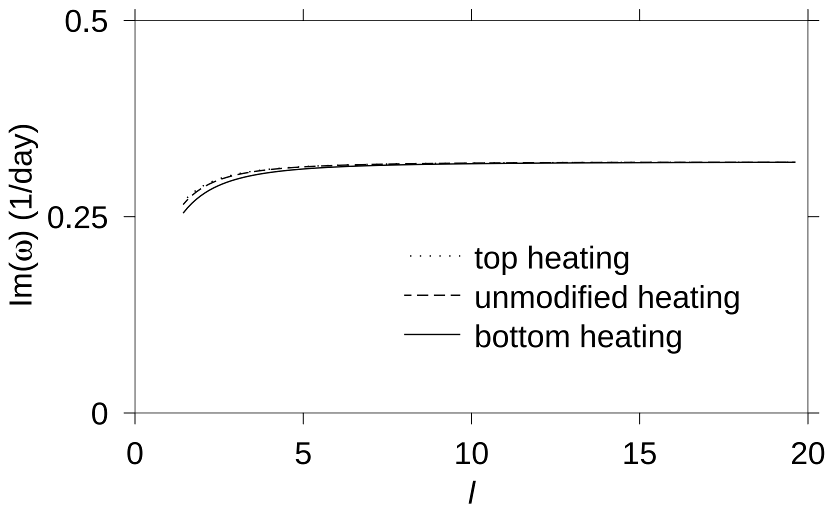

Figure 5: Growth rate of the moisture mode for fixed NGMS $= -0.1$ for different heating profiles, $\chi_t = 0$.

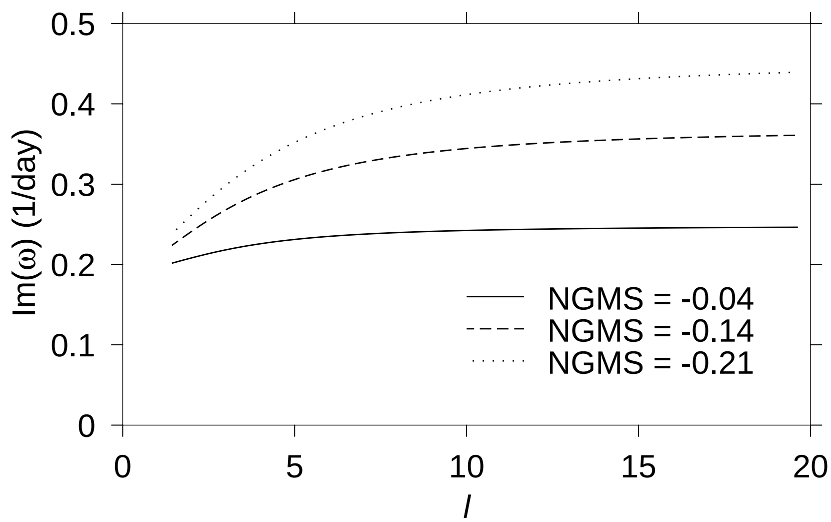

Figure 6: Growth rate of the moisture mode for different NGMS values for bottom-heavy heating profile.

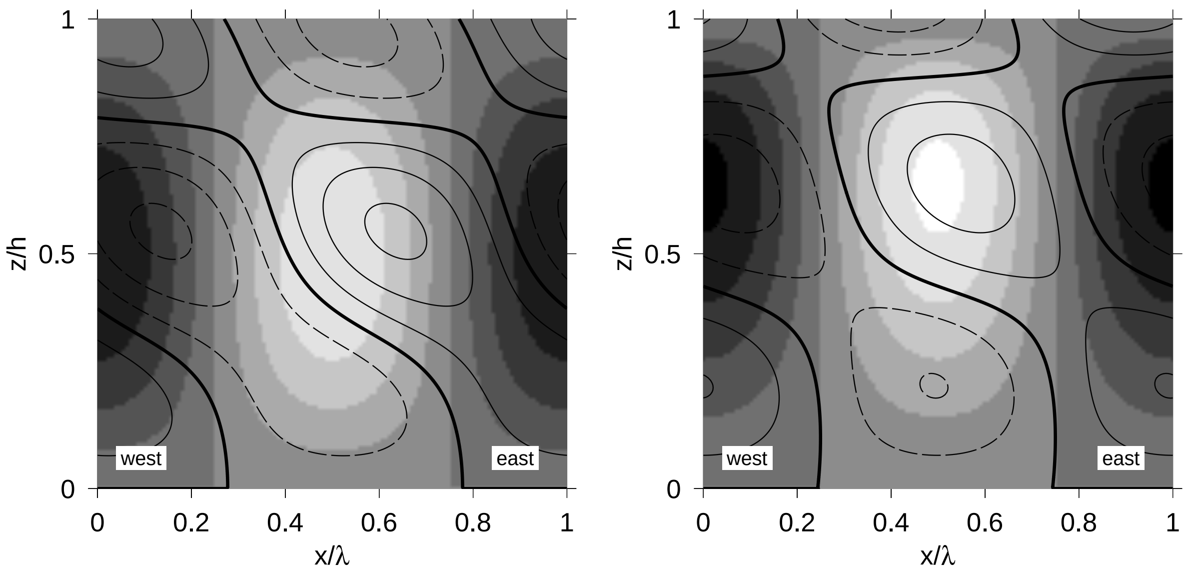

Figure 7: Heating anomaly and buoyancy perturbation for the convectively coupled gravity wave. Shading represents the heating anomaly, light shading positive and dark shading negative. Contours represent the buoyancy anomaly, solid lines positive and dashed lines negative. Left panel shows the unmodified heating profile and right panel shows top-heavy vertical heating profile.

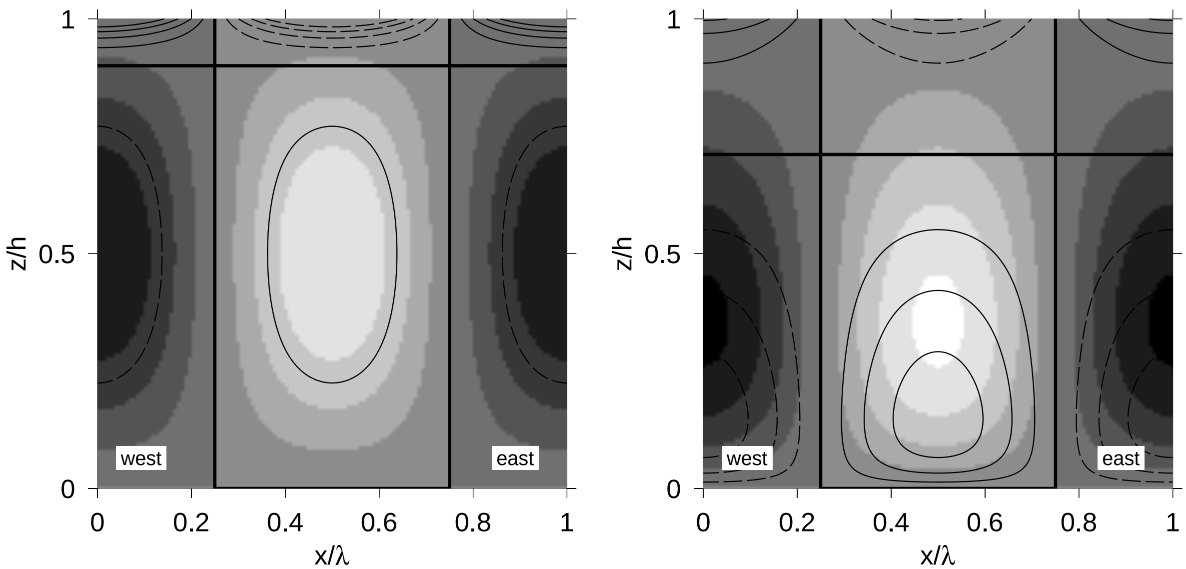

Figure 8: As in figure 7, heating anomaly and buoyancy perturbation, only for the moisture mode. Left panel shows the unmodified heating profile and right panel shows bottom-heavy vertical heating profile.

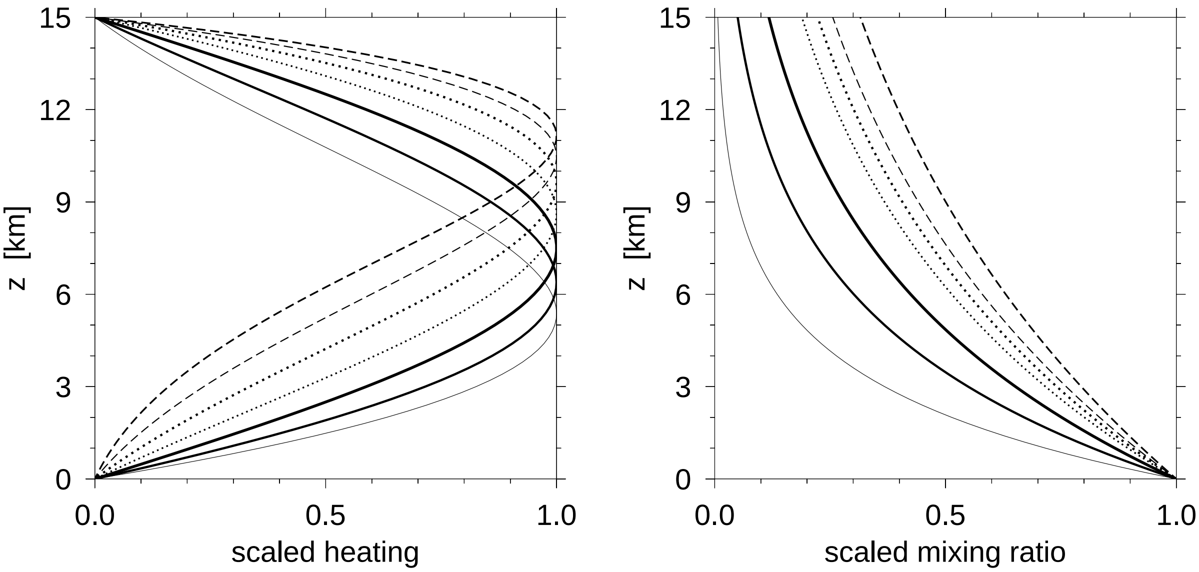

Figure 9: Scaled heating (left panel) and moisture (right panel) profiles as a function of height used for numerical model runs.

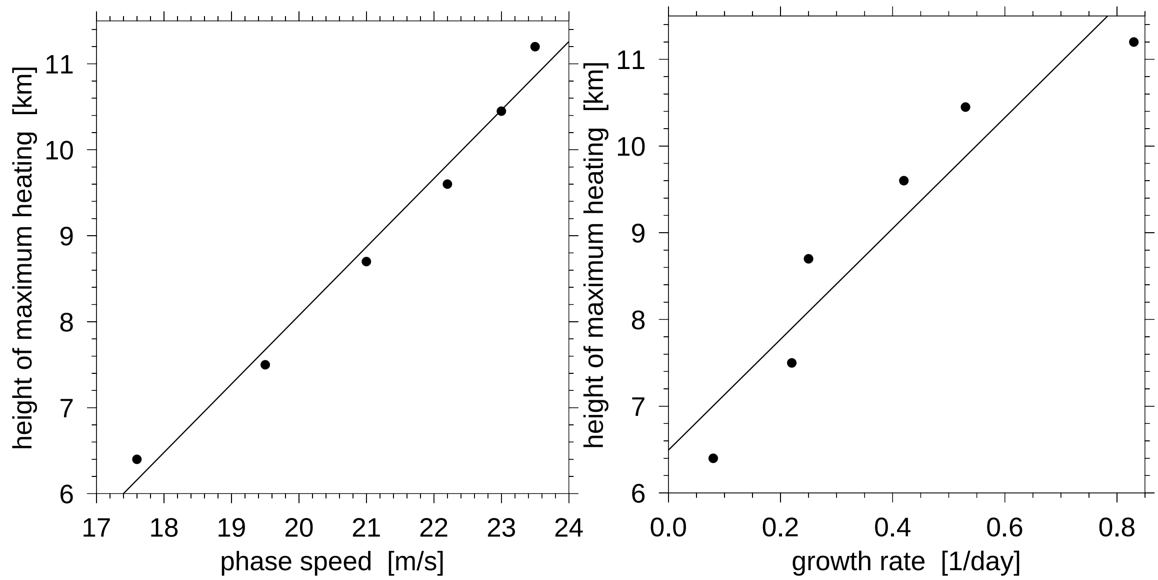

Figure 10: Left panel shows the phase speed for the convectively coupled gravity waves as a function of maximum heating height while right panel shows their growth rate.

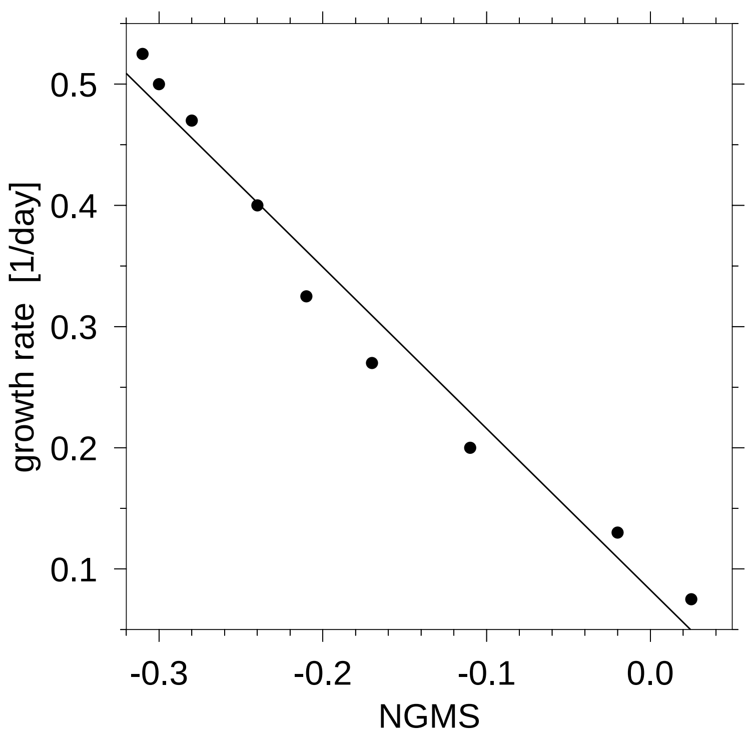

Figure 11: Growth rate for a moisture mode as a function of NGMS.

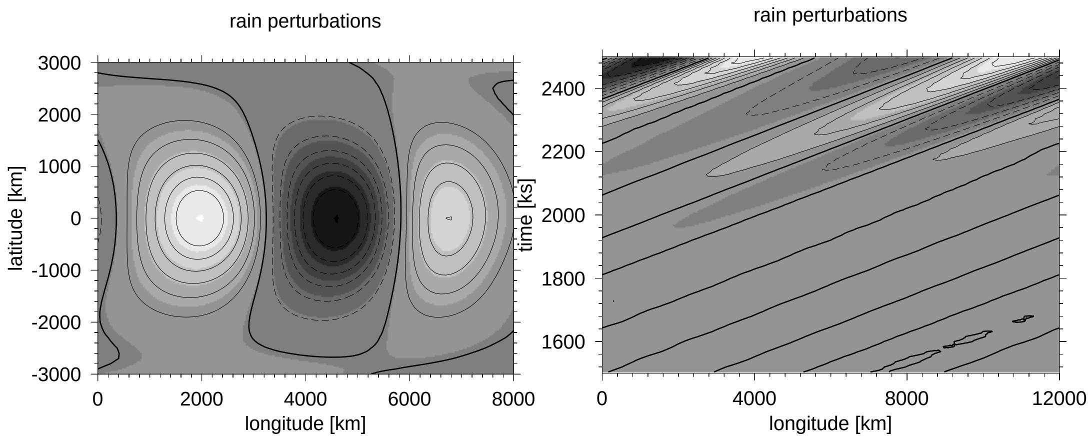

Figure 12: Convectively coupled Kelvin wave: left panel shows a snapshot of rainfall perturbations at the surface while right panel shows Hövmoller diagram of rainfall at the equator. The bold lines are zero contours, solid lines represent positive values and dashed lines represent negative values.

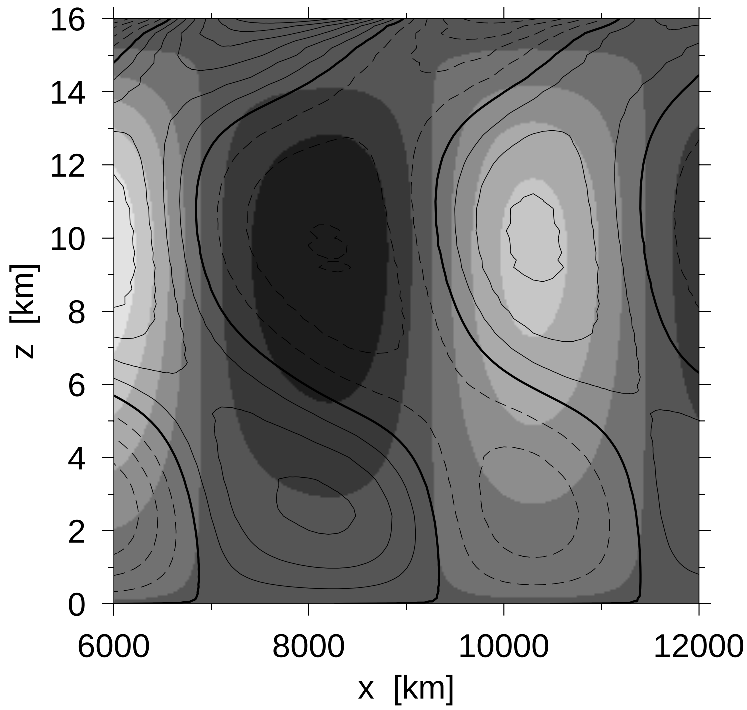

Figure 13: Vertical structure of the convectively coupled Kelvin wave along the equator in the numerical model. The heating anomaly is given in shading and potential temperature perturbation in contours. Light shading represents positive heating anomaly and dark negative. Solid contours represent positive potential temperature anomalies and dashed contours negative anomalies.

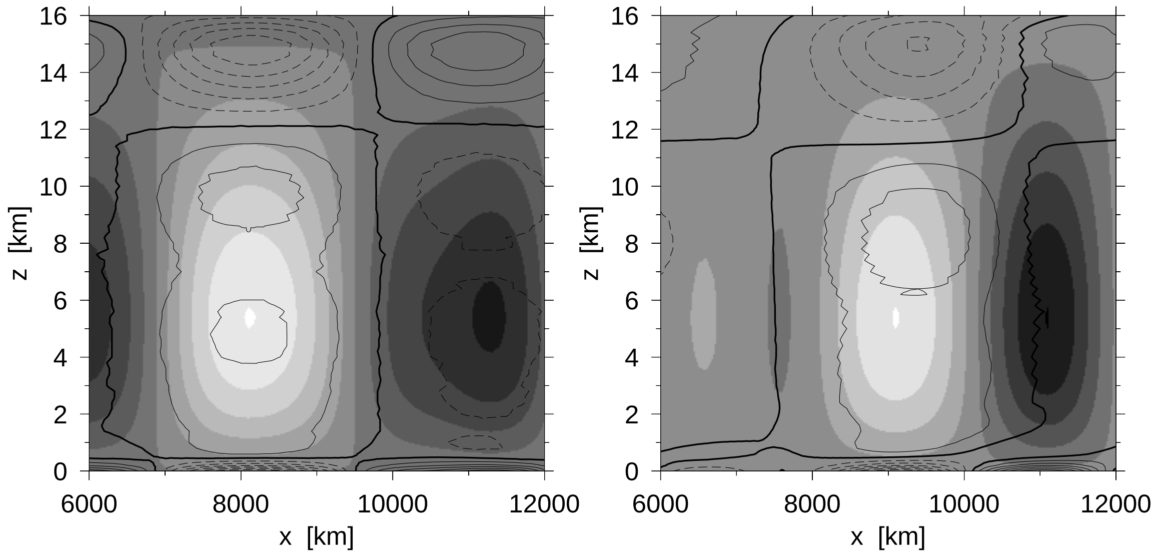

Figure 14: Heating anomaly and potential temperature as in figure 13, except for the moisture mode. The left panel shows vertical structure of the moisture mode in the two-dimensional case. The right panel shows the vertical structure along the equator in the three-dimensional case.